On Uncorrelated Inter-Monomer Förster Energy Transfer in Fenna–Matthews–Olson Complexes

Adam Kell[†,1], Anton Khmelnitskiy[†], Tonu Reinot[†,2], and Ryszard Jankowiak[†‡*]

[†]*Department of Chemistry and* [‡]*Department of Physics, Kansas State University, Manhattan, KS, USA*

Abstract

The Fenna-Matthews-Olson (FMO) light harvesting antenna protein of green sulfur bacteria is a long-studied pigment-protein complex which funnels energy from the chlorosome to the reaction center where photochemistry takes place. The structure of the FMO protein from *Chlorobaculum tepidum* is known as a homotrimeric complex containing eight bacteriochlorophyll *a* per monomer. Due to this structure FMO has strong intra-monomer and weak inter-monomer electronic coupling constants. While long-lived (sub-picosecond) coherences within a monomer has been a prevalent topic of study over the past decade, various experimental evidence supports the presence of subsequent inter-monomer energy transfer on a picosecond timescale. The latter is often neglected by most authors in recent years by considering only sub-picosecond timescales or assuming that the inter-monomer coupling between low-energy states is too weak to warrant consideration of the entire trimer. However, Förster theory predicts that energy transfer on the order of picoseconds is possible even for very weak (< 5 cm^{-1}) electronic coupling between chromophores. This work reviews experimental data (with a focus on emission and hole burned spectra) and simulations of exciton dynamics which demonstrate inter-monomer energy transfer. It is shown that the lowest energy 825 nm absorbance band cannot be properly described by a single excitonic state. The energy transfer through FMO is modeled by generalized Förster theory using a non-Markovian, reduced density matrix approach to describe the electronic structure. The disorder-averaged inter-monomer transfer times across the 825 nm band is about 27 ps. While only isolated FMO proteins are presented, the presence of inter-monomer energy transfer in the context of the overall photosystem is also briefly discussed.

---

[1]Present Address: Department of Chemistry and Chemical Biology, University of California–Merced, Merced, CA 95343, United States
[2]Present Address: 13025 Morehead, Chapel Hill, NC 27517, United States
*Corresponding Author: Ryszard Jankowiak, Department of Chemistry, Kansas State University, Manhattan, KS, United States; Tel: 785-532-6785; E-mail: ryszard@ksu.edu

I. Introduction. The Fenna-Matthews-Olson (FMO) light harvesting antenna protein of green sulfur bacteria is a long studied pigment-protein complex which funnels energy from the chlorosome to the reaction center (RC) where photochemistry takes place (Olson 2004; Milder et al. 2010). The structure of FMO is known as a homotrimeric complex (C_3 symmetry), containing eight bacteriochlorophyll (BChl) *a* per monomer (Tronrud et al. 2009), however, BChl *a* 8, located at the monomer connection regions, often has partial occupancy (Wen et al. 2011). Several decades ago (Sauer 1975) it was postulated that pigments within the FMO monomers are likely strongly coupled, and that Förster-type energy transfer could occur between the clusters (i.e., the monomers of FMO). In fact, there is a remarkable amount of experimental and theoretical papers related to the topic of the excitonic structure of FMO, its vibrational environment, and the origin of measured long-lived quantum coherences (Engel et al. 2007; Panitchayangkoon et al. 2010; Savikhin, Buck, and Struve 1997) and simulated (Huo and Coker 2010; Ishizaki and Fleming 2009; Rebentrost, Mohseni, and Aspuru-Guzik 2009; Vlaming and Silbey 2012). The observed quantum effects have been suggested to be responsible for the very high efficiency of excitation energy transfer (EET) in photosynthetic antenna complexes (Engel et al. 2007).

While there are multiple assignments of pigment site energies in the literature, it is well accepted that BChl *a* 3 and 4 contribute mostly to the lowest excitonic state in each monomer (Adolphs and Renger 2006; Adolphs and Renger 2008; Cho et al. 2005; Milder et al. 2010; Müh et al. 2007; Saer et al. 2017; Sarovar, Cheng, and Whaley 2011; Vlaming and Silbey 2012; Vulto et al. 1998; Wen et al. 2009). The composition of the initial state, i.e., which BChl molecule(s) receive excitation energy from the chlorosome baseplate, is still a matter of debate. Because of the orientation of FMO in relation to the RC, it was suggested that BChl 8 is the entry point of excitations from the chlorosome/baseplate system, with BChl 3 being the energy sink that transfers this energy to the P840 dimer of the RC (He et al. 2014; Wen et al 2009). However, the site energy of BChl 8 near 803-804 nm (12453-12438 cm^{-1}) and very weak coupling with other pigments most likely excludes such a scenario (Bina and Blankenship 2011; Kell, Blankenship, and Jankowiak 2016; Khmelnitskiy et al. 2018; Saer et al. 2017). Moreover, the calculations of Ritschel et al. (2011), showed that a relatively faster transfer is observed when initialization at BChls 1 or 6 is considered. Thus, it is likely that BChls 1 and 6 collect excitation from baseplate pigments, implying the existence of one or two (depending on modeling studies) relaxation pathways within a monomer (Brixner et al. 2005; Cho et al. 2005; Ishizaki and Fleming 2009; Moix et al. 2011). A single pathway with BChl 6 being the highest energy pigment is consistent with recent modeling studies of intact and intact/destabilized mixture FMO samples, where simultaneous fits of multiple optical spectra suggested that BChl 6 has the highest site energy followed by similar site energies of BChls 1 and 2 (Khmelnitskiy et al. 2018).

While previously published experimental data obtained by hole-burning (HB) spectroscopy (Johnson and Small 1991; Matsuzaki et al. 2000), fluorescence line-narrowing (FLN) (Johnson and Small 1991; Rätsep and Freiberg 2007a; Rätsep and Freiberg 2007b), pump-probe spectroscopy (Gulbinas et al. 1996; Savikhin and Struve 1994; Savikhin et al. 1994), photon echo experiments (Louwe and Aartsma 1997) and triplet-minus-singlet measurements (Louwe et al. 1997), as well as theoretical modeling (Herascu et al. 2014; Kell et al. 2014; Pearlstein 1992), have all suggested the possibility of inter-monomer energy transfer in FMO proteins, in simulations of excitonic structure (Caycedo-Soler et al. 2012), energy transfer pathways (Huo and Coker 2010; Moix et al. 2011; Wu et al. 2012; Wu et al. 2010) and non-Markovian noise correlation effects

(Mostame et al. 2012) often only the monomer is taken into account. Although the weak couplings between FMO subunits (i.e., the monomers) cause relatively small perturbation to the absorption spectrum, their influence should be magnified in the observed emission and hole-burned spectra due to a possible Förster-type energy transfer among the lowest energy states of the three monomers (Herascu et al. 2014; Kell et al. 2014; Savikhin, Buck, and Struve 1999). For example, both resonant and nonresonant HB spectra obtained for the 825 nm band of *Chlorobaculum* (*C.*) *tepidum* FMO are consistent with the presence of a relatively slow uncorrelated EET between the lowest energy states of the monomers of the trimer (mostly localized on BChl *a* 3), with a weak (~1-2 cm^{-1}) coupling between these states revealed via calculated emission spectra (see below) (Herascu et al. 2014). It was concluded that the nature of the 825 nm absorption band of the FMO trimer, contrary to the often accepted consensus (Caycedo-Soler et al. 2012; Milder et al. 2010), cannot be explained by a single transition. This simple model included both frequency dependent EET rate distributions and burning following EET, and provided reasonable fits of various optical spectra including resonant and nonresonant holes in the case of FMO complex. In subsequent works, (Kell, Blankenship, and Jankowiak 2016; Khmelnitskiy et al. 2018) briefly discussed below, a more advanced model that incorporated excitonic interactions was used to further demonstrate that the low-energy 825 nm band cannot be properly described by a single excitonic state.

This short review focuses on the nature of the lowest energy absorption band of FMO complexes from *C. tepidum*. We argue that after light induced coherences vanish, uncorrelated EET between the lowest exciton levels of each monomer takes place. The latter was neglected due to the fact that most authors in recent years have assumed that the inter-subunit coupling between BChl 3 is too weak to warrant consideration for the entire trimer. However, Förster theory (Förster 1948; Şener et al. 2011) predicts that energy transfer on the order of picoseconds is possible even for very weak (< 5 cm^{-1}) electronic coupling between chromophores.

II. Redfield and Förster Theories. Redfield theory is a second-order perturbative method that applies a Markovian approximation to describe energy relaxation in the limit of strong dipole-dipole coupling (Redfield 1957; Redfield 1965). To simulate various optical spectra, in modeling studies discussed below, we employ a non-Markovian density matrix approach (Renger and Marcus 2002a) for line shape calculations which utilizes a Redfield-like rate equation to describe relaxation between exciton states. Often the non-Markovian approach is still referred to simply as Redfield theory.

Frenkel Exciton Hamiltonian

The Frenkel Hamiltonian in the site representation is given by

$$\hat{H}_{site} = \sum_{m} \varepsilon_m \hat{A}_m^{\dagger} \hat{A}_m + \sum_{n \neq m} V_{mn} \hat{A}_m^{\dagger} \hat{A}_n$$

with ε_m the site energy (vertical transition energy) of pigment m, V_{mn} the inter-pigment coupling constant (both of the proceeding are in units of cm^{-1}), and $\hat{A}_m^{(\dagger)}$ the annihilation (creation) operator, respectively. Diagonalization of $\hat{H}_{site}$ yields the eigenvalues and eigenvectors of the excitonic system

$$\widehat{H}_{ex} = C^{-1}\widehat{H}_{site}C = \sum_{M} E_M \hat{A}_M^{\dagger}\hat{A}_M$$

where

$$\hat{A}_M^{(\dagger)} = \sum_{m} c_{mM}\hat{A}_m^{(\dagger)}$$

and c_{mM} are the elements of C (i.e., right eigenvector elements). In what follows lower- and upper-case subscripts ($m/n\ or\ M/N$) are used to denote chromophore and exciton excited states, respectively. In addition to excitonic interactions, electron-phonon coupling must be included to account for the influence of protein vibrations on the transition energies. The electron-phonon coupling is described by a phonon profile (spectral density) with overall coupling strength indicated by the reorganization energy (E_λ). Comparison of the magnitudes of V and E_λ determines which term can be treated perturbatively in the rate equation, leading to Redfield and Förster theories in the limits of strong and weak electronic dipole-dipole coupling, respectively (see below).

Phonon Profiles

The weighted phonon profile describes the electron-phonon coupling of an electronic transition with phonon modes ξ,

$$J(\tilde{\nu}) = \sum_{\xi} s_\xi \delta\left(\tilde{\nu} - \tilde{\nu}_\xi\right)$$

where s_ξ is the Huang-Rhys factor. It is assumed that the phonon profile can be approximated as a continuous function, which is chosen to be a log-normal distribution (Kell et al. 2013)

$$J_{ph}(\tilde{\nu}) = \frac{S_{ph}}{\tilde{\nu}\sigma\sqrt{2\pi}}\mathrm{e}^{-\frac{[\ln(\tilde{\nu}/\tilde{\nu}_c)]^2}{2\sigma}}$$

with the total molecular Huang-Rhys factor and reorganization energy defined as

$$S_{ph} = \int_0^\infty J_{ph}(\tilde{\nu})d\tilde{\nu}$$

and

$$E_\lambda = \int_0^\infty \tilde{\nu} J_{ph}(\tilde{\nu})d\tilde{\nu},$$

respectively. Similarly, a profile for the intra-molecular vibrational modes is given by

$$J_{vib}(\tilde{\nu}) = \sum_{v} \frac{s_v}{2\pi}\frac{\Gamma_v}{(\tilde{\nu} - \tilde{\nu}_v)^2 + \left(\frac{\Gamma_v}{2}\right)^2}$$

where the total vibrational Huang-Rhys factor is

$$S_{vib} = \int_0^\infty J_{vib}(\tilde{\nu})d\tilde{\nu}.$$

Temperature dependence is included in the profiles as

$$J(\tilde{\nu};T) = \big(1 + n(\tilde{\nu};T)\big)J(\tilde{\nu}) + n(-\tilde{\nu};T)J(-\tilde{\nu})$$

with the Bose-Einstein distribution

$$n(\tilde{\nu};T) = \frac{1}{\mathrm{e}^{\tilde{\nu}/kT} - 1}.$$

Note that the profiles are defined such that $J(\tilde{\nu} \leq 0) = 0$.

Rate Equations

When $V \gg E_\lambda$ (i.e., the strong coupling limit), excitonic relaxation is governed by coherent wave-like energy transfer. The non-Markovian rate is given by

$$k_{MN} = 2\pi\gamma_{MN}(E_M - E_N)^2 J(E_M - E_N;T)$$

where the delocalization parameter γ_{MN} depends on the eigenvector elements and a correlation radius

$$\gamma_{MN} = \sum_{m,n} c_{mM}c_{nM}c_{mN}c_{nN}\mathrm{e}^{-\frac{R_{mn}}{R_c}}.$$

R_c can be set to zero for uncorrelated fluctuations, however, a value of 5 Å has be elucidated from pump-probe data of Photosystem I (Renger and Marcus 2002b) and applied to FMO (Adolphs and Renger 2006). In the limit of weak coupling ($V \ll E_\lambda$) EET can modeled as incoherent hopping between localized excited states with a rate described by the Förster rate equation

$$k_{mn} = 2\pi|V_{mn}|^2 \int D'_m(\tilde{\nu})D_n(\tilde{\nu})d\tilde{\nu}$$

with the fluorescence (D') and absorption (D) line shape functions (see below).

Often for photosynthetic pigment-protein complexes $V \sim E_\lambda$, and a distinction of either the strong- or weak-coupling limit is not clearly defined. Here, an extension of Förster theory (so-called generalized Förster theory) is considered, where the excitonic system is divided into domains of strongly-coupled pigments. Intra-domain dynamics are simulated with Redfield theory, while inter-domain energy transfer is assumed to proceed via incoherent hopping described by the Förster equation (Raszewski and Renger 2008; Renger and Holzwarth 2008). In practice, for generalized Förster theory domains are determined by setting certain off-diagonal elements of the

Hamiltonian to zero, thus restricting the extent of exciton delocalization. In a simple approximation we assume all couplings smaller than a critical value (V_c, on the order of E_λ) should be zeroed.

The equations regarding the non-Markovian approach for exciton delocalization and intra-domain energy transfer are detailed elsewhere (Renger and Marcus 2002a). Here, the excitonic line shape function which includes the reorganization shift and lifetime broadening is given for completeness

$$D_M^{(\prime)}(\tilde{\nu}) = \int \mathrm{e}^{\pm 2\pi\mathrm{i}(\tilde{\nu}-\tilde{\nu}_M)\tau+\gamma_{MM}\left(G_{ph}(\tau)-G_{ph}(0)\right)-\pi\Gamma_M|\tau|}d\tau.$$

with ± corresponding to absorbance and fluorescence, respectively. Note that, due to dynamic localization (Hall et al. 2016; Renger et al. 2011), only the phonon profile effects the Redfield rate and intra-molecular vibrational modes are not considered for exciton line shapes $D_M^{(\prime)}$. Instead, the absorbance line shape function for localized vibrations is given by

$$D_m(\tilde{\nu}) = \int \mathrm{e}^{2\pi\mathrm{i}(\tilde{\nu}-\varepsilon_m+E_\lambda)\tau+G_{ph}(\tau)-G_{ph}(0)}\left(\mathrm{e}^{G_{vib}(\tau)}-1\right)d\tau,$$

$G(\tau)$ is the Fourier transform of the phonon or vibrational profiles. The line shape function in this form does not include the 0-0 (purely electronic in terms of intra-molecular vibrations) transition, which is taken into account in the excitonic line shape. The fluorescence vibrational line shape describes fluorescence from an exciton state to a vibrationally excited state of the ground electronic state,

$$D'_{m,M}(\tilde{\nu}) = \int \mathrm{e}^{-2\pi\mathrm{i}(\tilde{\nu}-\tilde{\nu}_M)\tau+G_{ph}(\tau)-G_{ph}(0)}\left(\mathrm{e}^{G_{vib}(\tau)}-1\right)d\tau.$$

Note that if all pigments have the same spectral densities, then the index m is unnecessary. The spectral overlap between delocalized excitonic state and localized vibrationally excited state contributes to the inter-domain transfer rate, thus both line shape functions enter the final generalized Förster rate equation.

For calculations of Förster rates (Renger and Holzwarth 2008; Renger et al. 2011) the coupling constants between two exciton states in domains a and b are given in terms of the inter-pigment constants as

$$V_{M_aN_b} = \sum_{m_a,n_b} c_{m_aM_a}c_{n_bN_b}V_{m_an_b}$$

while the coupling between an exciton state and a localized vibrational state is

$$V_{M_an_b} = \sum_{m_a} c_{m_aM_a}V_{m_an_b}$$

and enter into the Förster equation for exciton-exciton transfer

$$k_{M_aN_b} = 2\pi\left|V_{M_aN_b}\right|^2 \int D'_{M_a}(\tilde{\nu}) D_{N_b}(\tilde{\nu}) d\tilde{\nu} + 2\pi \sum_{n_b} \left|c_{n_bN_b}\right|^2 \left|V_{M_an_b}\right|^2 \int D'_{M_a}(\tilde{\nu}) D_{n_b}(\tilde{\nu}) d\tilde{\nu} + 2\pi \sum_{m_a} \left|c_{m_aM_a}\right|^2 \left|V_{m_aN_b}\right|^2 \int D'_{m_a,M_a}(\tilde{\nu}) D_{N_b}(\tilde{\nu}) d\tilde{\nu}.$$

Finally, the transfer rate between domains is given by a Boltzmann-weighted sum of the exciton energy transfer rates

$$k_{ab} = \sum_{M_a,N_b} \frac{e^{-E_{M_a}/kT}}{\sum_{K_a} e^{-E_{K_a}/kT}} k_{M_aN_b}.$$

III. On the Complex Nature of the 825 nm Exciton Band in the FMO Protein Complex. Below, Figure 1 shows the structure of *C. tepidum* FMO trimer (PDB ID: 3ENI) (Tronrud et al. 2009), which is used to calculate electronic coupling constants. The coupling constant between BChl 3 and 4 (the lowest energy pigments within a monomer) is –53.5 cm^{-1} when calculated using the TrEsp method (Madjet et al. 2006) and assuming a Q_y transition dipole strength of 25.2 D^2 (effective dipole strength includes the influence of the dielectric constant). In this case the coupling between BChl 3 pigments and BChl 4 pigments located in various monomers is –2.5 and 2.5 cm^{-1}, respectively. Frame B of Figure 1 shows the 825 nm absorption band (grey curve) and four resonant HB spectra (curves a–d, respectively). The shapes of the HB spectra clearly indicate the presence of downward energy transfer between FMO monomers. That is, low-energy satellite hole features are significantly more enhanced than would be warranted if EET was not present. The narrow, deepest holes are the resonant zero-phonon holes (ZPHs) coincident with λ_B, with pseudo- and real-phonon sideband holes (PSBHs) located ~22 cm^{-1} to the red and the blue, respectively. A similar phonon frequency of 22 cm^{-1} was observed by Matsuzaki et al. (2000) in FMO complexes from *Prosthecochloris* (*Pr.*) *aestuarii*. The bleaching to the lower energies with respect to the ZPHs is indicative of energy acceptors, not purely the pseudo-PSBHs as would be expected if the band was composed of a single exciton state, demonstrating that downward the EET within the 825 nm band is present. Thus, downward EET is observed, as pigments in different sub-states are burned due to direct transfer from the highest energy pigment subpopulation to the lowest energy subpopulation.

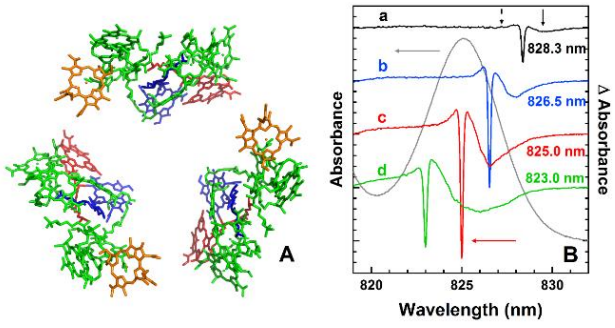

Figure 1. *Frame A*: structure of the FMO trimer showing the orientation of BChl *a* pigments. BChl *a* 3, 4 and 8 are colored blue, red and orange, respectively. *Frame B*: 5 K resonant HB spectra burned within the 825 nm band. Spectra a–d were obtained with λ_B = 828.3, 826.5, 825.0 and 823.0 nm, respectively, and are shifted for clarity. The dashed and solid arrows mark the real- and pseudo-PSBHs, respectively, while the red arrow indicates (as an example) the intense ZPH for curve c. The grey curve is the absorption band. Adapted from Kell et al. (2014).

All three subunits (i.e., FMO monomers) in the trimer are identical with identical site distribution functions (SDFs). Thus, due to diagonal energy disorder and uncorrelated EET between monomers, calculations for the entire FMO trimer would produce 24 different disorder-averaged excitonic states. That is, trimeric organization leads to a triple splitting of each disorder-averaged excitonic state of the monomer. Summation of excitonic energy "triplets" gives eight "effective" excitonic states of the isolated monomer (data not shown). In a first approximation, the lowest energy state of each monomer can be assumed to be localized on BChl 3 (i.e., neglecting excitonic interactions with the remaining pigments). The corresponding transition dipole moment can be determined from the crystal structure. The 825 nm band and resulting sub-bands calculated for this model are shown in Figure 2. That is, the subpopulations of the 825 nm band of FMO calculated (for simplicity) for trimer of BChl 3 only including phonon contribution. This is why three states 1-3, plotted in Figure 2 as green, blue, and red lines, respectively, contribute to the 825 nm absorption band. (The electron-phonon coupling is taken into account by a lognormal phonon spectral density (Kell et al. 2014) with the following parameters are used in simulations: Huang-Rhys factor S = 0.34, site-energy of all three BChls 3 is 12115 cm^{-1}, the coupling matrix element V_{33} = –3 cm^{-1}, and inhomogeneous broadening Γ_{inh} = 65 cm^{-1}). The three sub-band in Figure 2 correspond to: *i)* the lowest energy trap pigments with two donors (band 1); *ii)* pigments with one donor and one acceptor (band 2); and *iii)* the highest energy pigments with two acceptor pigments (band 3). Emission originates from band 1 (vide infra) which plays a role of the lowest energy trap. That is, due to disorder and EET sub-band 1 corresponds to the lowest energy state in the trimer that cannot transfer energy in isolated FMO complexes. The black curve in Figure 2 is the experimental absorption spectrum of wild-type FMO.

Formatted: Font: Times New Roman

Formatted: Font: Times New Roman

Formatted: Font: Times New Roman

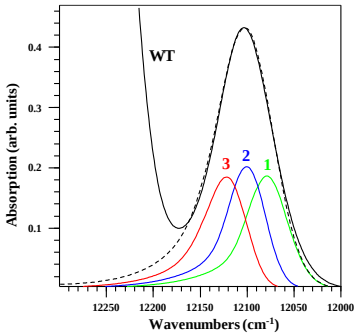

Figure 2. Calculated 825 nm band (dashed curve) for a trimer of BChl 3 only including phonon contribution. Each BChl 3 corresponds to a different FMO monomer (see text for details). In this case the trimeric organization with the same SDF for each BChl 3 leads to a triple splitting of the 825 nm absorption band.

The fluorescence spectrum can be simulated for the BChl 3 trimer while varying V_{33} (Herascu et al. 2014). Figure 3 shows the results of fluorescence simulations for this model. The curves in frame A correspond to the fluorescence origin bands (no phonons) calculated for weak coupling ($|V|$ = 0 – 3 cm^{-1}). The $V_{\_}$ = 0 case is identical to considering only a single monomer. As the coupling increases, sub-band 1 (no energy acceptors in isolated FMO) shifts to the red. Frame B shows simulated fluorescence spectra compared to the experimental 5 K spectrum. The data is well-described by $|V|$ = 0.9 cm^{-1}. This is slightly smaller than the value calculated from the crystal structure ($|V|$ = 2.5 cm^{-1}), but likely reflects errors due to the absence of excitonic interactions. However, the result is clear that the low-temperature steady-state fluorescence cannot be explained by a single monomer. Also, it cannot be entirely excluded that some fluorescence from sub-band 2 occurs, which is not taken into account here (see also discussion below for Figure 6).

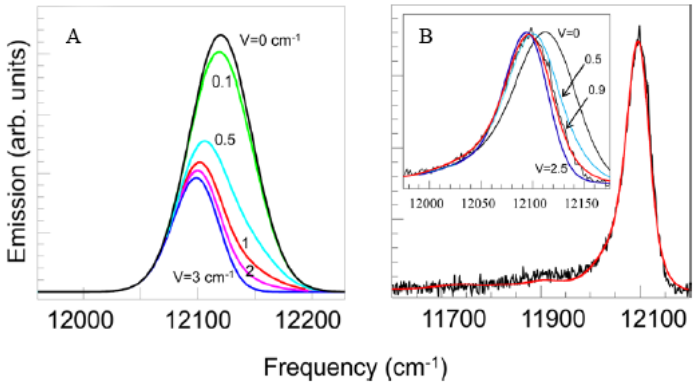

Figure 3. Calculated fluorescence origin bands (*frame A*) and fluorescence spectra (*frame B*) for the BChl 3 trimer with various coupling constants. A best fit to the experimental spectrum occurs for $|V|$ = 0.9 cm^{-1}. Adapted from Herascu et al. (2014).

As seen from Figure 4, fluorescence line-narrowed (FLN) spectra are consistent with the steady-state (non-line-narrowed) fluorescence. The vibronically excited spectra reveal only weak zero-phonon lines (ZPLs) superimposed on a broad fluorescence origin band, largely resulting from uncorrelated EET to the relatively long-lived emitting state. These results agree with vibronically excited FLN spectra reported for the FMO complex of *Pr. aestuarii* (Johnson and Small 1991).

Formatted: Font: Times New Roman

Formatted: Font: Times New Roman

Formatted: Font: Times New Roman

Formatted: Font: Times New Roman

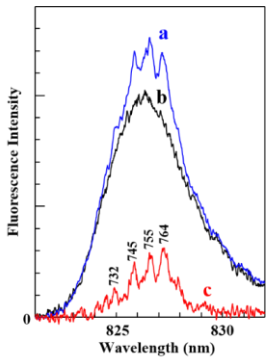

Figure 4. FLN (curve a) and non-line-narrowed fluorescence (curve b) spectra obtained for λ_{ex} = 778.0 and 496.5 nm, respectively, for *C. tepidum* FMO. The difference curve c = (a – b) reveals sharp ZPLs resulting from excitation resonant to the vibronic region. Numbers correspond to the excited state vibrational energies in cm^{-1} (unpublished data).

Distributions of Förster transfer times for pigments contributing to sub-band 2 (frame A) and sub-band 3 (frame B), where only BChls 3 are considered, are given in Figure 5. The distribution of transfer times shown in Figure 5 are calculated with Förster theory for V_{33} = –2.5 cm^{-1}. While the average relaxation time for sub-band 2 (positioned at 825.6 nm) is 70.0 ps, the distribution peaks at 32 ps. Likewise, the average and peak times for sub-band 3 are 41.3 and 20 ps, respectively. Previously reported experimental (high-resolution) resonant holes burned at λ_B = 822.8/824.8 nm (in *Pr. aestuarii*) and 823.0/825.0 nm (in *C. tepidum*) also suggested the presence of downward energy transfer in the 825 nm absorption band (Matsuzaki et al. 2000; Rätsep, Blankenship, and Small 1999). In those papers, the observed average relaxation time of 37 ps, i.e., EET time obtained from λ_B = 823.0 nm, is in reasonable agreement with Figure 5, in particular, when the distribution of EET times is taken into account. However, it is difficult to estimate the average relaxation time for the middle of the 825 nm band (i.e., λ_B = 825.0 nm), as at this wavelength there are contributions from sub-bands 2 and 3, as well as the trap states that do not transfer energy (i.e., sub-band 1).

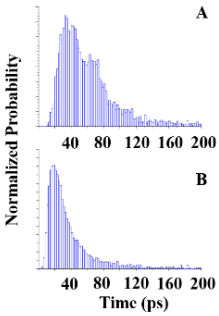

Figure 5. Distributions of Förster transfer times for pigments contributing to sub-band 2 (frame A) and sub-band 3 (frame B). Obtained for V_{33} = –2.5 cm^{-1} (i.e., the inter-monomer coupling between BChls 3).

The probabilities are normalized over 50 000 iterations (i.e., the sum of all probabilities is 1). Adapted from Kell et al. (2014).

The lowest energy BChl 3 is most strongly coupled to BChl 4, and both mostly contribute to the lowest energy absorption band near 825 nm (i.e., BChls 3 and 4 contribute about 85% and 15%, respectively (Kell et al. 2014; Khmelnitskiy et al. 2018)). So below we consider excitonic effects for a trimer of BChls 3 and 4 (in the absence of intra-molecular vibrations). That is, only two lowest energy BChls per monomer are included in modeling studies reported below. Frames A and B in Figure 6 show results obtained with the presence and absence of uncorrelated EET between FMO monomers, respectively. Here for simplicity we only show the low-energy part of the experimental and simulated absorption, emission, and HB spectra. In these simulations we also assumed that the lowest states of all three FMO monomers have the same SDFs. The solid (black) spectra correspond to the experimental absorption, emission and the persistent nonresonant HB spectra. The corresponding noisy red (frame A) and blue (frame B) curves are the calculated spectra. Intra-monomer interactions were modeled using Redfield theory (Renger and Marcus 2002a) with Förster energy transfer occurring between lowest energy molecules of various monomers. The grey spectra of frame A are the calculated states, which correspond to sub-bands 1-3 for the 825 nm band.

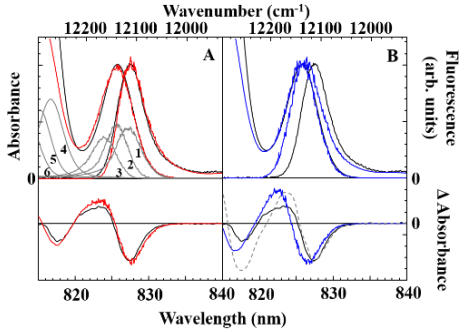

Figure 6. *Frame A*: Calculated (red) absorption, emission and HB (λ_B = 496.5 nm) spectra for a trimer model with EET compared to experiment (black). Grey curves are the calculated exciton states. *Frame B*: Spectra calculated assuming no EET between monomers (blue) compared to experiment (black). The grey dashed curve is the calculated HB spectrum assuming no 60 cm^{-1} shift after burning. HB spectra are offset for clarity. Adapted from Kell et al. (2014).

Formatted: Font: Italic

Note that only simulations shown in frame A are consistent with the experimental data, clearly indicating that the pigments contributing to sub-band 1 are burned first, as HB yield depends on the excited state lifetime. However, a partial bleaching of sub-band 2 cannot be entirely excluded. That is, some bleaching of higher-energy pigments occurs because their HB yield is small but not zero; and once some sub-band 1 pigments experience HB, pigments that used to contribute to sub-band 2 become lowest energy, and their HB yield increases. For more details and the Hamiltonian used for this for reduced structural model of FMO from *C. tepidum* (see Kell et al. 2014).

The monomer calculations (frame B) cannot account for the positions of nonresonant holes nor the emission spectrum, which is also too broad (consistent with Figure 3). The grey dashed curve in frame B of Figure 6 is the calculated HB spectrum assuming no 60 cm^{-1} shift due to a tier of the protein energy landscape (Herascu et al. 2014; Kell et al. 2014). The calculated emission (frame A) is slightly redshifted due to the assumption that only the lowest state emits. However, the experimental emission spectrum could also possess a small contribution from a fraction of pigments contributing to sub-band 2, because for small coupling and, for example, EET on the order of 100 ps, sub-band 2 could also emit directly, albeit with significantly reduced probability, even if sub-band 1 is not bleached.

Next, expanding on the above results, low-temperature optical spectra for the entire 24 pigment FMO trimer are modeled using a combination of non-Markovian Redfield and generalized Förster theories (Khmelnitskiy et al. 2018). The results are shown in Figure 7 along with spectral contributions of the eight BChls. The phonon profile (Kell, Blankenship, and Jankowiak 2016) and Huang-Rhys factor (S_{ph} = 0.4) are taken from the literature, as well as the intra-molecular vibrational modes (Rätsep and Freiberg 2007a). BChl site energies and inhomogeneous full-widths-at-half-maxima are optimized as free parameters. The fits (solid lines) shown in frame A describe the low-temperature data (filled curves) very well. BChl *a* 3 is the most red-shifted pigment and contributes 84.3% to the lowest energy exciton state with 12.3% contribution from BChl 4 (Khmelnitskiy et al. 2018). The latter pigment contributes mostly (43.3%) to the second exciton state at ~12264 cm^{-1}. As BChl 6 is located near the baseplate (Wen et al. 2009), it has the highest site energy and is the main contributor (57.2%) to the highest energy exciton state; with a small contribution from the remaining pigments. For more details, see Khmelnitskiy et al. (2018).

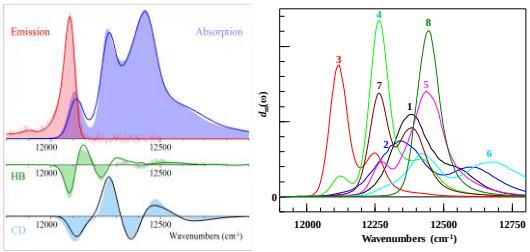

Figure 7. *Left frame*: Calculated low temperature (5 K) absorption (dark blue solid line), emission (red), low-fluence NRHB (green) spectra, and 6 K CD (black solid line, Vulto et al. 1998) compared to measured spectra (filled curves) for WT_I FMO trimers. *Right frame*: BChls 1-8 contributions to the calculated absorption spectrum shown in the left frame. Adapted from Khmelnitskiy et al. (2018).

Also in this case the 825 nm band is contributed to by three sub-bands (1-3) similar in shape to those presented in Figure 6 (frame A). The resulting energy transfer times from 3 →1, 2 →1, and 3 →2, are given in Table 1. The times are somewhat shorter than for the simple model presented above and discussed in Kell et al. (2014), as the excitonic interactions slightly change the electronic couplings and transition dipole moments of the lowest energy states. Additionally, the inclusion of energy transfer via vibrationally excited states increases the disorder-averaged inter-domain EET rates by approximately 40%. The calculated EET times between monomers agree well with other experimental data (vide infra).

Table 1. Energy transfer times between the three sub-bands contributing to the 825 nm band.

Sub-band EET	τ_{EET} (ps)
3→2	17
2→1	16
3→1	47

For example, the 37 ps component was found in the kinetic measurements for FMO complexes (*Pr. aestuarii*) that was attributed to energy transfer between subunits of the FMO trimer (Pearlstein 1992; Vulto, Streltsov, and Aartsma 1997). The previously observed time-dependent redshift of the FMO emission spectrum (Freiberg et al. 1997), where the ~30 ps time constant was observed (and related to energy transfer in the protein trimer between monomer subunits), is also consistent with our modeling studies. Finally, other studies which focused on slower processes taking place in FMO complexes, both at room and 77 K temperatures, found that a complete spectral equilibration in FMO proteins occurs in about 26 ps (Gulbinas et al. 1996). The latter time constant is likely due to equilibration within the trimer caused by the uncorrelated EET discussed above, again in good agreement with our results, where the calculated disorder-averaged τ_{EET} across the 825 nm band is about 27 ps.

The current analysis focuses on isolated FMO complexes at low-temperature (5 K), but provides some insight into energy trapping in the photosystem of green sulfur bacteria; as FMO transfers energy directly to the RC core complex. While there are still open questions about the structure of the RC core, there is strong evidence that there are about two FMO complexes positioned on the cytoplamic side of the RC (He et al. 2014; Rémigy et al. 1999). Experimental 2D electronic spectra assigned a 17 ps time to FMO → RC EET (Dostál, Pšenčík, and Zigmantas 2016). This suggests that inter-monomer EET competes with and possibly limits FMO → RC energy transfer. At the very least, inter-monomer transfer can occur before FMO → RC EET even in the intact photosystem. Previous comparison of emission spectra showed that FMO fluorescence is similar in both isolated samples and the chlorosome/FMO/RC system (Kell et al. 2015), suggesting that both stages of energy transfer through FMO (femtosecond intra-monomer relaxation and picosecond inter-monomer transfer) are part of the energy transport chain in the photosystem of green sulfur bacterium. However, transient absorption measurements on a FMO/RCC system could not difnitively assign a FMO → RC transfer time due to spectral overlap of BChls bound to each protein and an inherent inability to initially excite only FMO (He et al. 2015). Thus, future work is needed to further investigate energy trasnfer to the RC.

IV. Concluding Remarks. In summary, low-temperature emission and HB spectra, as well as modeling studies, clearly indicate the existence of uncorrelated EET within the sub-states of the lowest energy absorption band of the FMO complex. Each trimer has three identical monomers connected by Förster-type EET. Therefore, the 825 nm band in the FMO protein cannot be explained by a single electronic transition, in agreement with numerous experimental data. Moreover, the dependence of the Huang-Rhys factor across the 825 nm band (Rätsep and Freiberg 2007a; Rätsep and Freiberg 2007b), as well as the shapes of FLN and resonant HB spectra, are likely caused by uncorrelated EET between monomers of the FMO trimer. Thus, the observed fluorescence and hole burning originate from the lowest energy excitonic sub-state. This

uncorrelated EET between monomers is preceded by downward energy relaxation in each monomer on a sub-picosecond to about one picosecond time scale. The presence of subsequent inter-monomer energy transfer is not unique to isolated proteins, but likely occurs even when the RC is present.

Acknowledgments

This work was supported by the Chemical Sciences, Geosciences and Biosciences Division, Office of Basic Energy Sciences, Office of Science, U.S. Department of Energy (Grants No. DE-SC0006678 to R.J.).

References

Adolphs, Julian, and Thomas Renger. 2006. How proteins trigger excitation energy transfer in the FMO complex of green sulfur bacteria. *Biophysical Journal* 91 (8): 2778–97.

Adolphs, Julian, Frank Müh, Mohamed El-Amine Madjet, and Thomas Renger. 2008. Calculation of pigment transition energies in the FMO protein: From simplicity to complexity and back. *Photosynthesis Research* 95 (2): 197-209, 211.

Bina, David, and Robert E. Blankenship. 2013. Chemical oxidation of the FMO antenna protein from *Chlorobaculum tepidum*. *Photosynthesis Research* 116 (1): 11-9.

Brixner, Tobias, Jens Stenger, Harsha M. Vaswani, Minhaeng Cho, Robert E. Blankenship and Graham R. Fleming. 2005. Two-dimensional spectroscopy of electronic couplings in photosynthesis. *Nature* 434 (7033): 625-8.

Caycedo-Soler, Felipe, Alex W. Chin, Javier Almeida, Susana F. Huelga, Martin B. Plenio. 2012. The nature of the low energy band of the Fenna-Matthews-Olson complex: Vibronic signatures. *The Journal of Chemical Physics* 136 (15): 155102.

Cho, Minhaeng, Harsha M. Vaswani, Tobias Brixner, Jens Stenger, and Graham R. Fleming. 2005. Exciton analysis in 2D electronic spectroscopy. *The Journal of Physical Chemistry B* 109 (21): 10542-56.

Dostál, Jakub, Jakub Pšenčík, and Donatas Zigmantas. 2016. *In situ* mapping of the energy flow through the entire photosynthetic apparatus. *Nature Chemistry* 8 (7): 705–10.

Engel, Gregory S., Tessa R. Calhoun, Elizabeth L. Read, Tae-Kyu Ahn, Tomáš Mančal, Yuan-Chung Cheng, Robert E. Blankenship, and Graham R. Fleming. 2007. Evidence for wavelike energy transfer through quantum coherence in photosynthetic systems. *Nature* 446 (7137): 782-6.

Förster, Theodor. 1948. Zwischenmolekulare energiewanderung und fluoreszenz. *Annalen der Physik* 437 (1-2): 55–75.

Freiberg, Arvi, Su Lin, Kõu Timpmann, and Robert E. Blankenship. 1997. Exciton dynamics in FMO bacteriochlorophyll protein at low temperatures. *The Journal of Ohysical Chemistry B* 191 (37): 7211–20.

Gulbinas, Vidmantas, Leonas Valkunas, Darius Kuciauskas, Evaldas Katilius, Vladas Liuolia, Wenli Zhou, and Robert E. Blankenship. 1996. Singlet–singlet annihilation and local heating in FMO complexes. *The Journal of Physical Chemistry* 100 (45): 17950–6.

Hall, Jeremy, Thomas Renger, Rafael Picorel, and Elmars Krausz. 2016. Circularly polarized luminescence spectroscopy reveals low-energy excited states and dynamic localization of vibronic transitions in CP43. *Biochimica et Biophysica Acta - Bioenergetics* 1857 (1): 115–28.

He, Guannan, Dariusz M. Niedzwiedzki, Gregory S. Orf, Hao Zhang, and Robert E. Blankenship. 2015 Dynamics of energy and electron transfer in the FMO-reaction center core complex from the photosynthetic green sulfur bacterium *Chlorobaculum tepidum*. *The Journal of Physical Chemistry B* 119 (26): 8321–9.

He, Guannan, Hao Zhang, Jeremy D. King, and Robert E. Blankenship. 2014. Structural analysis of the homodimeric reaction center complex from the photosynthetic green sulfur bacterium *Chlorobaculum tepidum*. *Biochemistry* 53 (30): 4924–30.

Herascu, Nicoleta, Adam Kell, Khem Acharya, Ryszard Jankowiak, Robert E. Blankenship, and Valter Zazubovich. 2014. Modeling of various optical spectra in the presence of slow excitation energy transfer in dimers and trimers with weak inter-pigment coupling: FMO as an example. *The Journal of Physical Chemistry B* 118 (8): 2032–40.

Huo, Pengfei, and David F. Coker. 2010. Iterative linearized density matrix propagation for modeling coherent excitation energy transfer in photosynthetic light harvesting. *The Journal of Chemical Physics* 133 (18): 184108.

Ishizaki, Akihito, and Graham R. Fleming. 2009. Theoretical examination of quantum coherence in a photosynthetic system at physiological temperature. *Proceedings of the National Academy of Sciences of the United States of America* 106 (41): 17255–60.

Johnson, Stephen G., Gerald J. Small. 1991. Excited-state structure and energy-transfer dynamics of the bacteriochlorophyll *a* antenna complex from *Prosthecochloris aestuarii*. *The Journal of Physical Chemistry* 95 (1): 471–9.

Kell, Adam, Khem Acharya, Valter Zazubovich, and Ryszard Jankowiak. 2014. On the controversial nature of the 825 nm exciton band in the FMO protein complex. *The Journal of Physical Chemistry Letters* 5 (8): 1450–6.

Kell, Adam, Robert E. Blankenship, and Ryszard Jankowiak. 2016. Effect of spectral density shapes on the excitonic structure and dynamics of the Fenna–Matthews–Olson trimer from *Chlorobaculum tepidum*. *The Journal of Physical Chemistry A* 120 (31): 6146–54.

Kell, Adam, Jinhai Chen, Mahboobe Jassas, Joseph Kuo-Hsiang Tang, and Ryszard Jankowiak. 2015. Alternative excitonic structure in the baseplate (BChl *a*–CsmA complex) of the chlorosome from *Chlorobaculum tepidum*. *The Journal of Physical Chemistry Letters* 6 (14): 2702–7.

Kell, Adam, Ximao Feng, Mike Reppert, and Ryszard Jankowiak. 2013. On the shape of the phonon spectral density in photosynthetic complexes. *The Journal of Physical Chemistry B* 117 (24): 7317–23.

Khmelnitskiy, Anton, Adam Kell, Tonu Reinot, Rafael G. Saer, Robert E. Blankenship, and Ryszard Jankowiak. 2018. Energy landscape of the intact and destabilized FMO antennas from *C. tepidum* and the L122Q mutant: Low temperature spectroscopy and modeling study. *Biochimica et Biophysica Acta - Bioenergetics* 1859 (3): 165–73, (5): 409.

Louwe, Robert J. W., and Thijs J. Aartsma. 1997. On the nature of energy transfer at low temperatures in the BChl *a* pigment-protein complex of green sulfur bacteria. *The Journal of Physical Chemistry B* 101 (37): 7221–6.

Louwe, Robert J. W., Jacobien Vrieze, Thijs J. Aartsma, and Arnold J. Hoff. 1997. Toward an integral interpretation of the optical steady-state spectra of the FMO-complex of *Prosthecochloris aestuarii*. 1. An investigation with linear-dichroic absorbance-detected magnetic resonance. *The Journal of Physical Chemistry B* 101 (51): 11273–9.

Madjet, Mohamed E., Ayjamal Abdurahman, and Thomas Renger. 2006. Intermolecular coulomb couplings from ab initio electrostatic potentials: Application to optical transitions of strongly coupled pigments in photosynthetic antennae and reaction centers. *The Journal of Physical Chemistry B* 110 (34): 17268–81.

Matsuzaki, Satoshi, Valter Zazubovich, Margus Rätsep, John M. Hayes, and Gerald J. Small. 2000. Energy transfer kinetics and low energy vibrational structure of the three lowest energy Q_y-states of the Fenna-Matthews-Olson antenna complex. *The Journal of Physical Chemistry B* 104 (40): 9564–72.

Milder, Maaike T. W., Ben Brüggemann, Rienk van Grondelle, and Jennifer L. Herek. 2010. Revisiting the optical properties of the FMO protein. *Photosynthesis Research* 104 (2–3): 257–74.

Moix, Jeremy, Jianlan Wu, Pengfei Huo, David Coker, and Jianshu Cao. 2011. Efficient energy transfer in light-harvesting systems, III: The influence of the eighth bacteriochlorophyll on the dynamics and efficiency in FMO. *The Journal of Physical Chemistry Letters* 2 (24): 3045–52.

Mostame, Sarah, Patrick Rebentrost, Alexander Eisfeld, Andrew J. Kerman, Dimitris I. Tsomokos, and Alán Aspuru-Guzik. 2012. Quantum simulator of an open quantum system using superconducting qubits: Exciton transport in photosynthetic complexes. *New Journal of Physics* 14 (10): 105013.

Müh, Frank, Mohamed El-Amine Madjet, Julia Adolphs, Ayjamal Abdurahman, Björn Rabenstein, Hiroshi Ishikita, Ernst-Walter Knapp, and Thomas Renger. 2007. α-helices direct excitation energy flow in the Fenna-Matthews-Olson protein. *Proceedings of the National Academy of Sciences of the United States of America* 104 (43): 16862-7.

Olson, John M. 2004. The FMO protein. *Photosynthesis Research* 80 (1): 181-7.

Panitchayangkoon, Gitt, Dugan Hayes, Kelly A. Fransted, Justin R. Caram, Elad Harel, Jianzhong Wen, Robert E. Blankenship, Gregory S. Engel, and Graham R. Fleming. 2010. Long-lived quantum coherence in photosynthetic complexes at physiological temperature. *Proceedings of the National Academy of Sciences of the United States of America* 107 (29): 12766-70.

Pearlstein, Robert M. 1992. Theory of the optical spectra of the bacteriochlorophyll *a* antenna protein trimer from *Prosthecochloris aestuarii*. *Photosynthesis Research* 31 (3): 213–26.

Raszewski, Grzegorz, and Thomas Renger. 2008. Light Harvesting in Photosystem II core complexes is limited by the transfer to the trap: Can the core complex turn into a photoprotective mode? *Journal of the American Chemical Society* 130 (13): 4431–46.

Rätsep, Margus, and Arvi Freiberg. 2007a. Electron-phonon and vibronic couplings in the FMO bacteriochlorophyll *a* antenna complex studied by difference fluorescence line narrowing. *Journal of Luminescence* 127 (1): 251–9.

Rätsep, Margus, and Arvi Freiberg. 2007b. Unusual temperature quenching of bacteriochlorophyll *a* fluorescence in FMO antenna protein trimers. *Chemical Physics Letters* 434 (4–6): 306–11.

Rätsep, Margus, Robert E. Blankenship, and Gerald J. Small. 1999. Energy transfer and spectral dynamics of the three lowest energy Q_y-states of the Fenna-Matthews-Olson antenna complex. *The Journal of Physical Chemistry B* 103 (27): 5736–41.

Rebentrost, Patrick, Masoud Mohseni, and Alán Aspuru-Guzik. 2009. Role of quantum coherence and environmental fluctuations in chromophoric energy transport. *The Journal of Physical Chemistry B* 113 (29): 9942–7.

Redfield, Alfred G. 1957. On the theory of relaxation processes. *IBM Journal of Research and Development* 1 (1): 19–31.

Redfield, Alfred G. 1965. The theory of relaxation processes. *Advances in Magnetic Resonance* 1 (1): 1–32.

Rémigy, Hervé-W., Henning Stahlberg, Dimitrios Fotiadis, Shirley A. Müller, Bettina Wolpensinger, Andreas Engel, Günter Hauska, and Georgios Tsiotis. 1999. The reaction center complex from the green sulfur bacterium *Chlorobium tepidum*: A structural analysis by scanning transmission electron microscopy. *Journal of Molecular Biology* 290 (4): 851–8.

Renger, Thomas, and Alfred R. Holzwarth. 2008. Theory of excitation energy transfer and optical spectra of photosynthetic systems. In *Biophysical Techniques in Photosynthesis II*, edited by Thijs J. Aartsma, and Jörg Matysik, 421–43. Dordrecht: Springer.

Renger, Thomas, and Rudolph A. Marcus. 2002a. On the relation of protein dynamics and exciton relaxation in pigment-protein complexes: An estimation of the spectral density and a theory for the calculation of optical spectra. *The Journal of Chemical Physics* 116 (22): 9997–10019.

Renger, Thomas, and Rudolph A. Marcus. 2002b. Photophysical properties of PS-2 reaction centers and a discrepancy in exciton relaxation times. *The Journal of Physical Chemistry B* 106 (7): 1809–19.

Renger, Thomas, Mohamed E. Madjet, A Knorr, and Frank Müh. 2011. How the molecular structure determines the flow of excitation energy in plant light-harvesting complex II. *Journal of Plant Physiology* 168 (12): 1497–509.

Ritschel, Gerhard, Jan Roden, Walter T. Stunz, Alán Aspuru-Guzik, and Alexander Eisfeld. 2011. Absence of quantum oscillations and dependence on site energies in electronic excitation energy transfer in the Fenna–Matthews–Olson trimer. *The Journal of Physical Chemistry Letters* 2 (22): 2912–17.

Saer, Rafael G., Valentyn Stadnytskyi, Nikki C. Magdaong, Carrie Goodson, Sergei Savikhin, and Robert E. Blankenship. 2017. Probing the excitonic landscape of the *Chlorobaculum tepidum* Fenna-Matthews-Olson (FMO) complex: A mutagenesis approach. *Biochimica et Biophysica Acta - Bioenergetics* 1858 (4): 288-96.

Sarovar, Mohan, Yuan-Chung Cheng, and K. Birgitta Whaley. 2011. Environmental correlation effects on excitation energy transfer in photosynthetic light harvesting. *Physical Review E* 83 (1): 011906.

Sauer, Kenneth. 1975. Primary events and the trapping of energy. In *Bioenergetics of Photosynthesis*, edited by Govindjee, 115–81. New York: Academic.

Savikhin, Sergei, and Walter S. Struve. 1994. Ultrafast energy transfer in FMO trimers from the green bacterium *chlorobium tepidum*. *Biochemistry* 33 (37): 11200-8.

Savikhin, Sergei, Daniel R. Buck, and Walter S. Struve. 1997. Oscillating anisotropies in a bacteriochlorophyll protein: Evidence for quantum beating between exciton levels. *Chemical Physics* 223 (2): 303-12.

Savikhin, Sergei, Daniel R. Buck, and Walter S. Struve. 1999. The Fenna–Matthews–Olson protein: A strongly coupled photosynthetic antenna. In *Resonance Energy Transfer*, edited by David L. Andrews, and Andrey A. Demidov, 399 – 434. Chinchester: John Wiley & Sons.

Savikhin, Sergei, Wenli Zhou, Robert E. Blankenship, Walter S. Struve. 1994. Femtosecond energy transfer and spectral equilibration in bacteriochlorophyll *a*–protein antenna trimers from the green bacterium *Chlorobium tepidum*. *Biophysical Journal* 66 (1): 110–3.

Şener, Melih, Johan Strümpfer, Jen Hsin, Danielle Chandler, Simon Scheuring, C. Neil Hunter, and Klaus Schulten. 2011. Förster energy transfer theory as reflected in the structures of photosynthetic light-harvesting systems. *ChemPhysChem* 12 (3): 518–31.

Tronrud, Dale E., Jianzhong Wen, Leslie Gay, and Robert E. Blankenship. 2009. The structural basis for the difference in absorbance spectra for the FMO antenna protein from various green sulfur bacteria. *Photosynthesis Research* 100 (2): 79-87.

Vlaming, Sebastiaan, and Silbey, Robert J. 2012. Correlated intermolecular coupling fluctuations in photosynthetic complexes. *The Journal of Chemical Physics* 136 (5): 055102.

Vulto, Simone I. E., Michiel A. de Baat, Robert J. W. Louwe, Hjalmar P. Permentier, Tatjana Neef, Mette Miller, Herbert van Amerongen, and Thijs J. Aartsma. 1998. Exciton simulations of optical spectra of the FMO complex from the green sulfur bacterium *Chlorobium tepidum* at 6 K. *The Journal of Physical Chemistry B* 102 (47): 9577–82.

Vulto, Simone I. E., Alexander M. Streltsov, and Thijs J. Aartsma. 1997. Excited state energy relaxation in the FMO complexes of the green bacterium *Prosthecochloris aestuarii* at low temperatures. *The Journal of Physical Chemistry B* 101 (24): 4845–50.

Wen, Jianzhong, Hao Zhang, Michael L. Gross, and Robert E. Blankenship. 2009. Membrane orientation of the FMO antenna protein from *Chlorobaculum tepidum* as determined by mass spectrometry-based footprinting. *Proceedings of the National Academy of Sciences of the United States of America* 106 (15): 6134-9.

Wen, Jianzhong, Hao Zhang, Michael L. Gross, and Robert E. Blankenship. 2011. Native electrospray mass spectrometry reveals the nature and stoichiometry of pigments in the FMO photosynthetic antenna protein. *Biochemistry* 50 (17): 3502–11.

Wu, Jianlan, Fan Liu, Jian Ma, Robert J. Silbey, and Jianshu Cao. 2012. Efficient energy transfer in light-harvesting systems: Quantum-classical comparison, flux network, and robustness analysis. *The Journal of Chemical Physics* 137 (17): 174111.

Wu, Jianlan, Fan Liu, Young Shen, Jianshu Cao, and Robert J. Silbey. 2010. Efficient energy transfer in light-harvesting systems, I: Optimal temperature, reorganization energy and spatial–temporal correlations. *New Journal of Physics* 12 (10): 105012.